Journal of
Synchrotron Radiation

ISSN 0909-0495

Received 18 January 2011
Accepted 17 March 2011

Atomic absorption background of Ba in EXAFS analysis of $BaFe_{12}O_{19}$ nanoparticles

Jana Padežnik Gomilšek,[a]* Alojz Kodre,[b,c] Iztok Arčon,[c,d] Simone de Panfilis[e] and Darko Makovec[c]

[a]Faculty of Mechanical Engineering, University of Maribor, Smetanova 17, SI-2000 Maribor, Slovenia, [b]Faculty of Mathematics and Physics, University of Ljubljana, Jadranska 19, Slovenia, [c]J. Stefan Institute, Jamova 39, SI-1000 Ljubljana, Slovenia, [d]University of Nova Gorica, Vipavska 13, SI-5000 Nova Gorica, Slovenia, and [e]Dipartimento di Fisica, Università di Roma 'La Sapienza', P. le Aldo Moro 5, I-00185 Roma, Italy. E-mail: jana.padeznik@uni-mb.si

The approximate barium X-ray atomic absorption in the energy region of *L*-edges is reconstructed from the absorption spectrum of an aqueous solution of $BaCl_2$. The result is corroborated by comparison with pure atomic absorption spectra of neighbour elements Xe and Cs. The application of the atomic absorption signal as a proper EXAFS background is demonstrated and discussed in the analysis of Ba hexaferrite nanoparticles with a very weak structural signal. The essential gain is found in the decrease of uncertainty intervals of structural parameters and their correlations. A simple analytical model of the absorption background for the practical EXAFS analysis is demonstrated.

Keywords: X-ray absorption; hydrated barium ion L_3-edge EXAFS; Ba L_3 atomic absorption background; Ba hexaferrite nanoparticle EXAFS; [2*p*4*d*] resonant multi-electron excitation; analytical approximation to atomic background.

1. Introduction

In molecular or solid-state aggregates the X-ray photoabsorption cross section of an atom is modified by the interference of the photoelectron wavefunction with wavelets scattered from the neighbour atoms. The resulting modulation of the cross section, as a function of photon energy, is termed the structural signal, or extended X-ray absorption fine structure (EXAFS). It is strong in well ordered samples where scattering contributions of several shells of neighbour atoms add coherently. On a sample of free atoms, on the other hand, the pure atomic cross section without structural signal is measured. It consists of smooth contributions of electron shells or subshells (K, L_1, L_2, L_3, ...), each of them apparent by their ionization threshold, *i.e.* the absorption edge, and a subsequent slow decrease with increasing photon energy. Within a few hundred eV above an edge, small sharp features of collective excitations [multi-electron photoexcitations (MPEs)] of the atomic system are superposed upon the smooth absorption spectrum. The experimental data on MPEs provide useful information for advanced atomic models, particularly on the effects of electron correlation. The atomic absorption of an element is also useful as the atomic absorption background (AAB) for EXAFS analysis. In well ordered samples the EXAFS signal is stronger than the AAB by an order of magnitude, so the exact shape of the AAB is not essential; it is routinely approximated by a spline, generated from the low-r Fourier components of the signal. In strongly disordered samples with a weak structural signal, the EXAFS and AAB may be of comparable strength, and a useful structural signal is obtained only when the proper AAB is removed from the data.

With the exception of noble-gas elements, which are inherently monatomic, a sample of free atoms of an element is difficult to prepare and maintain in stability for a spectroscopy measurement of the AAB. In most experiments so far, prevalently monatomic metal vapours have been used, and the experimentally most accessible K-edge energy region has been studied (Padežnik Gomilšek *et al.*, 2001, 2003; Kodre *et al.*, 2002, 2006; Mihelič *et al.*, 2002). Experiments in the L-edge region, which are more difficult owing to the lower penetration power of soft X-rays, have been published only for Cs and Hg (Kodre *et al.*, 2010; Filipponi *et al.*, 1993). Useful data on MPEs can be obtained by other techniques such as emission spectroscopy (Žitnik *et al.*, 2007).

Since only a few metals are sufficiently volatile, with boiling points below 1300 K, for the experiment, alternative methods for the measurement of the AAB or its reasonable approximation have been developed (Padežnik Gomilšek *et al.*, 2009; Prešeren *et al.*, 2001). In absorption spectra of samples with a weak and simple EXAFS, the structural signal can be removed by modelling of the atomic neighbourhood (Li *et al.*, 1992), preferably in a crosswise iteration of two or more independent samples. A sequence of the AAB in a contiguous series of

elements from Ga to Rb has been determined in this way (Padežnik Gomilšek *et al.*, 1999; Kodre *et al.*, 1999).

The need for a specific AAB for the L_3 EXAFS of Ba arose recently in an investigation of crystal forms of barium hexaferrite, $BaFe_{12}O_{19}$, prepared by a modification of the hydrothermal method (Primc *et al.*, 2009). Ba hexaferrite is one of the most commonly used materials in magnetic recording and in millimetre-wave applications. For stable suspensions, such as in ferrofluids or for electrophoretic deposition of hexaferrite films, ultrafine nanoparticles with sizes below ∼20 nm are required. Usually, hexaferrite is formed at elevated temperatures above 900 K, which makes the synthesis of ultrafine nanoparticles very difficult. In a hydrothermal synthesis in the presence of a high excess of hydroxyl ions, formation temperatures as low as 370 K can be reached, with a good yield of discoid ultrafine nanoparticles of diameter ∼10 nm and thickness ∼3 nm. At increased synthesis temperatures these ultrafine nanoparticles tend to grow through secondary recrystallization or Ostwald ripening, but the process can be effectively blocked by addition of a surfactant, oleic acid. Since the thickness corresponds to no more than two unit-cell heights, only the lateral symmetry of the structure can be determined by X-ray diffraction, and EXAFS is resorted to for characterization of the product (Makovec *et al.*, 2011). Two batches of discoid ultrafine nanoparticles of comparable size were studied: nanoparticles HF synthesized hydrothermally at 423 K without surfactant and strongly agglomerated, and nanoparticles OA synthesized at 513 K in the presence of oleic acid to prevent agglomeration. Both displayed a strongly suppressed EXAFS signal in comparison with the signal of the Ba hexaferrite ceramic standard, obtained by repeated calcination of stoichiometric amounts of Fe_2O_3 and $BaCO_3$ powders in air (Fig. 1).

The structural signal of the nanoparticles is strongly suppressed beyond $k \simeq 5.5$ Å^{-1} by the deficient coordination and by a large Debye–Waller width owing to the large disorder. As a result, the neighbour shells beyond the first contribute very little. The analysis of the signal is hampered by the short L_3 range, cut off by the subsequent L_2 edge at $k \simeq 10$ Å^{-1}. In addition, the peculiarly large amplitude of the signal at $k = 5.5$ Å^{-1}, equal to that of the standard, is a hint of a large contribution of multi-electron excitations, in this case the resonant transition to the [2*p*4*d*] state. Apparently the two constituents of the absorption spectrum, the structural signal and the AAB, are of comparable strength, and a proper AAB, instead of a spline construction, is required in the preliminary steps of EXAFS analysis (Makovec *et al.*, 2011).

Since the atomic absorption of Ba vapour has not been measured yet, the approximate barium L_3 AAB is determined on a Ba sample with a weak and simple EXAFS, the aqueous solution of Ba^{2+} ions. The neighbourhood of the ion has been studied in detail earlier using a combination of EXAFS and molecular dynamics (D'Angelo *et al.*, 1996), with a similar goal: to construct a Ba AAB. Several conclusions of the study have been adopted in the analysis of our data.

Recently, we have also measured the proper *L*-edge atomic absorption on the preceding elements Xe and Cs (Kodre *et al.*, 2010). The results establish some trends of the AAB in the group of elements, providing a test for the approximate Ba AAB.

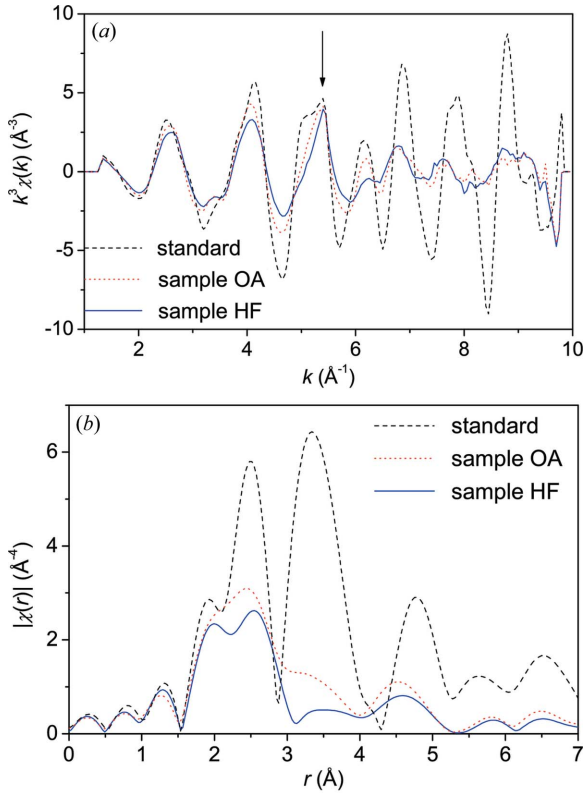

Figure 1
L_3 EXAFS of the $BaFe_{12}O_{19}$ ceramics and two batches of nanoparticles (OA and HF). The position of the 4*d* feature in the *k*-space is indicated by the arrow.

2. Experiment

An aqueous solution of $BaCl_2$ (0.35 mg $BaCl_2{\cdot}2H_2O$ in 2.6 mg H_2O, ∼0.5 *M*), providing a sample of quasi-free Ba^{2+} ions, *i.e.* ions with a strongly disordered neighbourhood, was prepared. An absorption spectrum of a ∼0.25 mm-thick layer of the solution between 0.3 mm-thick lucite windows in a liquid-absorption cell was measured at the BM29 station of ESRF, using a Si 111 monochromator with a resolution of ∼0.7 eV, and ionization detectors filled with 240 mbar, 1500 mbar and 2000 mbar N_2, respectively, and topped up with He to 2000 mbar. Beam harmonics were eliminated with a plane Si mirror and with active monochromator control. The energy scale of the monochromator was calibrated with a scan of the *K*-edge of a 4 µm-thick chromium foil (*K*-edge at 5989 eV).

In the scan over the entire *L* region (Fig. 2) from 5050 eV to 6500 eV a step of 1 eV was used, except for the 200 eV-wide edge regions which were covered with steps of 0.25 eV. The overload of the apex of the L_3 white line was tolerated for the sake of overall sensitivity of the scan, since the profile of the line could be reconstructed from its L_2 counterpart.

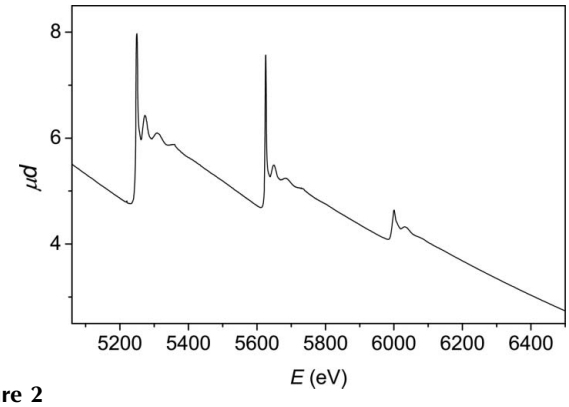

Figure 2
Panoramic view of the L-edge absorption of Ba^{2+} ions in aqueous solution. The sharp resonance at the L_3-edge is truncated by overload of the counting electronics.

3. Analysis

Fig. 2 shows a spectrum over the three L edges, with a short-range EXAFS signal above each edge; these provide at least two independent combinations of the structural signal and AAB. A rough approximation of the AAB can be prepared simply by the cancellation of the structural signals above the L_3- and L_1-edges, since the phase shifts of the two in the k-space, according to EXAFS theory, differ almost exactly by π. The fact is demonstrated in Fig. 3 with opposite oscillations of the two normalized structural signals. The sum of the two is not exactly the required L_3 AAB but rather the sum of L_3 and L_1 AAB. Nevertheless, the remainder shows a strong peak at the position of the resonant transition to a double core vacancy state $[2(p,s)4d]$ at $\sim$5.5 Å^{-1}, conspicuous already in each edge segment itself.

To extract the AAB, or an approximation thereof, a two-stage iterative procedure is adopted. The structural signal to be removed from the measured data is obtained by modelling the simple EXAFS of the hydrated ion with two neighbour shells, the oxygen and hydrogen atoms, following the results of the molecular dynamics of D'Angelo *et al.* (1996). In the first stage the parameters of the *Ifeffit* model (Ravel & Newville, 2005; Rehr & Albers, 2000), the coordination number, the Debye–Waller width and the scattering length, however, are determined by the least-squares fit to the measured EXAFS signal. Third moments of the path length distribution were introduced initially as parameters to account for its strong apparent asymmetry but became superficial in the second stage of the procedure.

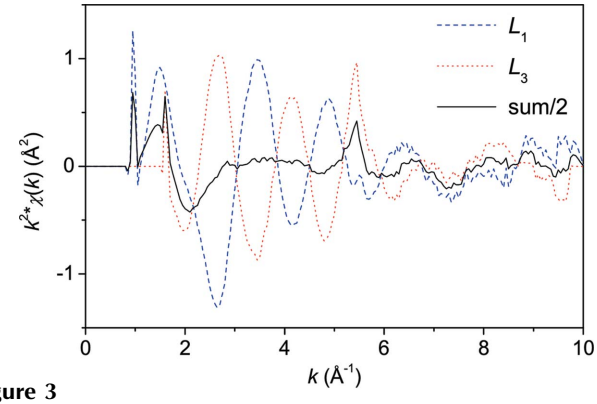

Figure 3
The k^2-weighted EXAFS signals above the L_1- and L_3-edges of Ba^{2+} ions in aqueous solution, normalized to the respective edge jumps. The opposite phases of the signals ensure almost total cancellation over a wide interval, 2.7–6.3 Å^{-1}, between the XANES residuals on the low-k side and noise on the high-k side, displaying the non-structural 4d resonance at $\sim$5.5 Å^{-1}.

A simultaneous modelling of the signal at the three edges is used to improve the accuracy of the result and the stability of the relaxation. The three model signals use common structural parameters but separate edge shifts E_0. The calculation shows that the hydrogen contribution is minute, its parameters are weakly defined, subject to large correlations. For the overall stability of the fit the coordination number of the hydrogen shell is constrained to double the value of the oxygen coordination, with a single $\Delta r/r$ parameter for the relative correction to the Ba—O and Ba—H distances. The Debye–Waller width of the hydrogen shell is kept constant at the value borrowed from D'Angelo *et al.* (1996).

The best-fit model of the L_3 structural signal in the k-range 2.8–9.5 Å^{-1}, with the standard quality-of-the-fit measure r-factor of 4.5%, is shown in r-space (Fig. 4*a*). The best-fit parameters are shown in Table 1. The O coordination number is considerably below the generally accepted value of 9 resulting also from molecular dynamics simulations, but close to the experimental value of 7.4 from D'Angelo *et al.* (1996). The low coordination stems also from adoption of the unit

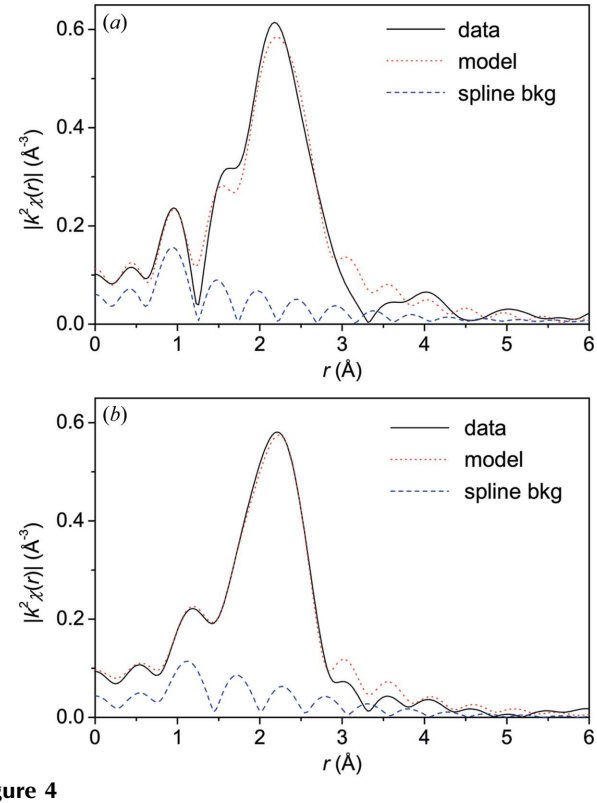

Figure 4
Fourier transforms of the k^2-weighted L_3 EXAFS of hydrated Ba ions (*a*) as measured and (*b*) after removal of the 4d resonance, together with a two-shell fit. The spline background of *Ifeffit* constructed from the harmonic components below r = 1.3 Å and relaxed in the fit is also shown.

Table 1
Best-fit parameters of the two-shell EXAFS model of the hydrated Ba^{2+} ions determined on the raw data and after removal of the 4*d* feature.

The uncertainty intervals in units of the last decimal place are given in parentheses. The values in brackets are constrained in the fit.

	First stage		Second stage	
	O	H	O	H
N	8.3 (1.0)	{16.7}	6.4 (8)	{12.8}
r (Å)	2.80 (1)	3.46 (2)	2.80 (2)	3.46 (2)
σ^2 (Å^2)	0.016 (3)	{0.03}	0.014 (3)	{0.03}
E_0 (eV)	−3.9 (0.9)		−3.1 (1.1)	
r-factor	0.045		0.0065	

photoelectron coherence factor, $S_0^2 = 1$, owing to lack of a reliable experimental value.

After the removal of the best-fit model signal from the measured absorption signal in E-space, the initial approximations to the three L-subshell AABs are obtained. Besides the dominant feature of the sharp resonance conspicuous also in the Ba-ferrite spectra, they exhibit some smooth trends, amenable to a spline approximation, and some oscillations, residuals of the structural signal. It should be noted that the difference between the measured signal and the pure structural model by necessity also contains the spline background removed in the preparatory *Athena* stage of the *Ifeffit* package. The spline, constructed from the r-space signal components below r_{min}, cannot remove the resonance because of its broad Fourier spectrum.

In the second stage of the procedure the input data in the relaxation are corrected for the effect of the background resonance. Subtracting from the measured data a narrow stretch of the approximate background containing the resonance should improve the fit of the model and sharpen the relaxation of the parameters. One should not try, however, to subtract the entire background. The remainder, in that case, would be exactly the best-fit model of the first stage: if introduced as input EXAFS signal, the identical values of the parameters would be obtained. For the second stage, the segments of the backgrounds from 5.5 to 6 Å, suitably padded to reach zero at the ends of the interval, were subtracted from respective subshell spectra, and another simultaneous fit was performed. The quality of the fit, as conventionally measured by the r-factor, was greatly improved (Fig. 4*b*). With the removal of the atomic background components the EXAFS signal is much closer to the model. The main effect on the parameters is the 25% decrease of the coordination numbers while the radius of the shell remains unchanged. With further iterations of this stage the fit is not improved.

The residual, obtained by removing the improved fit from the measured signal, is the best approximation of the AAB, accessible by the present approach. The idea of Padežnik Gomilšek *et al.* (1999) that the isolation of an AAB requires at least two independent EXAFS spectra has been taken into account by using the three independent L-subshell spectra of hydrated Ba ions.

Recently, L atomic absorption spectra have been measured on monatomic Xe gas and Cs vapour (Kodre *et al.*, 2010). In these spectra, with very low noise and in the absence of the structural signal, the MPE can be discerned in full detail. Except for its relatively large noise level, the Ba AAB represents a reasonable continuation of the series (Fig. 5). In opposition to the conventional concave curvature of K absorption, the L_3 spectra comprise excitations which build a convex baseline. This anomaly of L_2 and L_3 absorption is known as the 'polarization effect' (Jitschin & Stotzel, 1998). After several attempts the curvature of the L absorption spectra was first successfully reconstructed in a RRPARC (relativistic random-phase approximation with relaxation, involving overlap integrals with continuum final state orbitals) calculation for Xe (Kutzner, 2004).

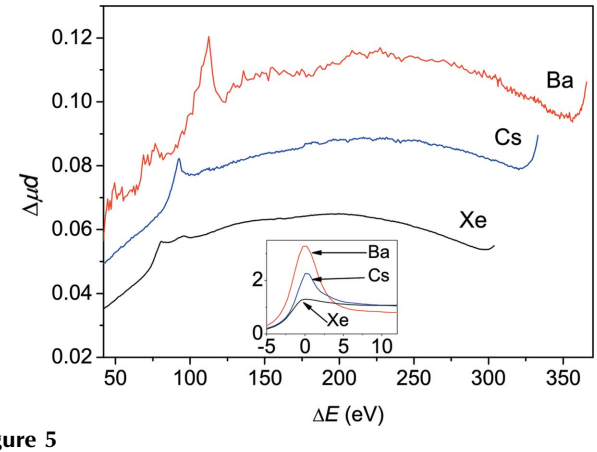

Figure 5
The proper L_3 atomic absorption of Xe and Cs together with the present result on Ba. The asymptotic downward trend of the absorption coefficient, recognizable in the high-energy side of Fig. 2, is removed as in Kodre *et al.* (2010). Inset: L_3-edge profiles with white lines of the elements on the same energy scale, as conjectural templates of 4*d* resonances. The Ba L_3-edge is reconstructed from the uncorrupted L_2-edge.

The most conspicuous feature of the AAB in this range of elements is the consecutive increase of the 4*d* resonance. It continues into the lanthanide series (Padežnik Gomilšek *et al.*, 2004; Ion *et al.*, 2010) following the increase of the strength of the [2*p*]4*d* resonance, the 'white line', at the L_3-edge. The parallel rise and fall of the two resonances has been formulated in a conjecture, by which the fingerprint of the entire group of 4*d* coexcitations, comprising the resonance [2*p*4*d*]5d^2 and the shake-up edge [2*p*4*d*]5*d*, is a tiny replica of the L_3-edge with the leading white line. The remaining channel within the MPE group, the shake-off [2*p*4*d*], is entirely inconspicuous at the threshold, with just a change of slope, and can be neglected in this similarity. The most salient support cases of the conjecture are the 4*d* features in lanthanides with different valence states (Solera *et al.*, 1995). Even within the same valence the feature (together with the L_3-edge profile) may change with ligands of different electron affinity.

4. Results

The application of the absorption background is demonstrated in a practical EXAFS analysis of the Ba ferrite nanoparticles of Fig. 1 with an extremely weak structural signal. A sample of

bulk Ba ferrite ceramics with a rich structural signal is analyzed alongside for comparison.

The unmodified EXAFS spectra are modelled with a *Feff* model built from the crystallographic data by Obradors *et al.* (1985), chosen among several sets compiled in the ICSD collection as the closest to the three samples. The model comprises single-scattering paths of two O shells (6 + 6 atoms), and three Fe shells (3 + 6 + 6) within a distance of 4 Å, the range of useful data for the nanoparticles. For a statistically significant fit the rich model requires a large number of independent points which the short *k*-range of the EXAFS signal cannot provide. Therefore, the spectra of the three samples are fitted jointly on a triple number of independent points, with some obvious constraints to reduce the number of parameters. Thus, the widths of the paths are varied directly but often constrained to a common value for two or three samples. The path lengths are varied through a single expansion parameter $\Delta r/r$ for each sample, with some individual path corrections where necessary. The coordination numbers are kept fixed at the model value for the bulk ceramics sample, with an adjustable factor for each of the elements in the nanoparticle samples. With 35 parameters, including the 3 × 7 parameters of *Athena* spline backgrounds, for 50 independent points of the data, a fit with an average *r*-factor of 0.022 can be obtained, with the maximum correlation between a pair of parameters of 94%.

Table 2
Structural parameters of the EXAFS model of the three Ba ferrite samples.

The values of the untreated (*a*) and AAB-corrected (*b*) signal are shown side by side for easier comparison. The uncertainty intervals in units of the last decimal place are given in parentheses. Values without error estimate are held fixed or constrained in the relaxation. $S_0^2 = 1$ is adopted.

			Standard		Sample OA		Sample HF	
		Obradors *et al.* (1985)	(*a*)	(*b*)	(*a*)	(*b*)	(*a*)	(*b*)
	E_0 (eV)		6.5 (1.1)	8.8 (3)	6.5	8.8 (3)	6.5	8.8 (3)
O1	N	6	4.4 (8)	5.3 (5)	5.0 (5)	4.8 (3)	4.1 (4)	3.7 (2)
	r (Å)	2.87	2.77 (3)	2.93 (3)	2.75 (3)	2.81 (3)	2.75	2.80 (3)
	σ^2 (10^{-4} Å^2)		44 (33)	150 (10)	57 (33)	50 (10)	57	50 (10)
O2	N	6	7.4 (8)	6.7 (5)	6.8 (5)	6.0 (3)	7.1 (8)	4.6 (3)
	r (Å)	2.95	2.94 (23)	2.93 (3)	2.96 (3)	3.01 (3)	2.96 (3)	2.99 (3)
	σ^2 (10^{-4} Å^2)		44 (33)	150 (10)	57 (33)	50 (10)	57 (33)	50 (10)
Fe1	N	3	3	3	0.4 (2)	0.4 (1)	–	–
	r (Å)	3.41	3.46 (5)	3.44 (3)	3.43 (5)	3.40 (3)	–	–
	σ^2 (10^{-4} Å^2)		95 (7)	89 (5)	95 (7)	72 (5)	–	–
Fe2	N	6	6	6	0.8 (4)	0.8 (2)	–	–
	r (Å)	3.67	3.69 (5)	3.70 (3)	3.69 (5)	3.67 (3)	–	–
	σ^2 (10^{-4} Å^2)		95 (7)	89 (5)	95 (7)	72 (5)	–	–
Fe3	N	6	6	6	0.8 (4)	0.8 (2)	–	–
	r (Å)	3.69	3.70 (5)	3.72 (3)	3.70 (5)	3.69 (3)	–	–
	σ^2 (10^{-4} Å^2)		95 (7)	89 (5)	95 (7)	72 (5)	–	–
r-factor			0.0060	0.0088	0.0307	0.0061	0.0281	0.0239

The same model is applied to the data from which the AAB of Fig. 5 is removed. There, an average *r*-factor of 0.013 is obtained with only 30 active parameters, so that the maximum correlation remains at 71%. The results of both fits are shown in Table 2, recalculated to standard path parameters N, r and σ^2 for clearer comparison. The shifts in individual values are not dramatic; the most significant change for practical structural interpretation is in the coordination numbers of oxygen shells, leading to a reorganization of the model O shells in the standard. More importantly, the uncertainty intervals of the variables are almost halved for the corrected data. The improvement is the result of the smaller correlation between parameters. In this way a smaller number of varied parameters leads to smaller error intervals. Apparently, the corrected data agree better with the model, so that fewer parameters are required: it seems that the non-structural components in the data 'pull' the fit away from the structural model. The fact is demonstrated graphically in Fig. 6, where fits of the unmodified and modified data are shown. The departure of the fit from the unmodified data is largest in the same region of the spectrum where the effect of the correction is the most pronounced, *i.e.* on the low-*r* side of the oxygen peak. The 'pull' enhances the splitting between the O shells and redistributes their amplitudes. After the removal of the AAB, the parameters return nearer to the crystallographic values. Incidentally, in the ceramic standard where the thermal treatment induces the relaxation to high symmetry, the splitting of the shells is practically removed, reinterpreted instead as an increase in the width of the shell. In any case, the short *k*-range of the data limits the spatial resolution to ∼0.15 Å, making the analysis only weakly sensitive to the splitting introduced by the crystallographic model.

When the experimental AAB is used for the correction, the noise level of the data is somewhat increased by the noise of the AAB. Instead, a smooth analytic approximation of the AAB, more convenient also for compilation, can be subtracted from the measured spectra. In a test, a fit of a Lorentzian resonance and arctan edge to the AAB as shown in Fig. 7 was used for the correction. The constants of the approximation, *i.e.* the amplitude A in units of L_3-edge jump, the width Γ and the energy position ΔE relative to the apex of the L_3 white line (E_3 = 5249 eV), are given in Table 3. The gain in the average improvement of parameter uncertainty is practically the same as that in Table 2. The Lorentzian alone contributes about 70% of the gain. An analytical arctan ansatz for the AAB has also been used by D'Angelo *et al.* (1996) in the standard form for the *GNXAS* code (Filipponi *et al.*, 1995), without the resonance term and with the constants adjusted in the best fit to the target spectrum.

The constants in Table 3 of the analytical approximation are obtained entirely by fit, adjusted for the simplest possible formula. A more precise treatment would yield a number of terms, representing the multiplet structure of the 4*d* MPE group, or at least the dominant $d_{3/2}$–$d_{5/2}$ splitting. This splitting is hidden in the width Γ of the resonance term, which is evidently much larger than the natural width, ∼3 eV, of the Ba

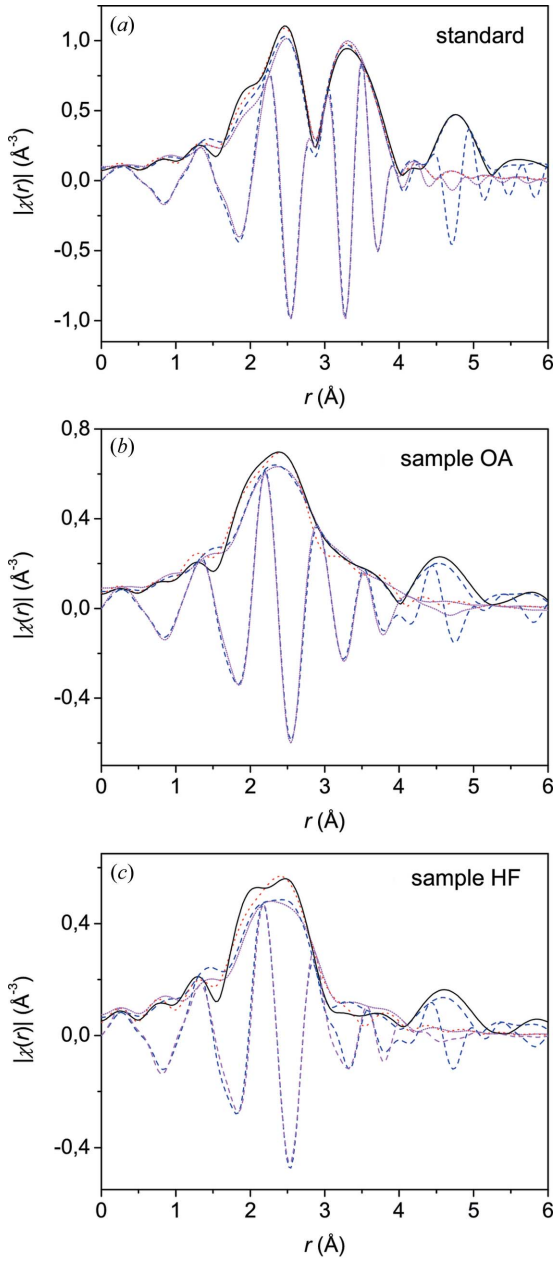

Figure 6
The amplitude and imaginary part of k^2-weighted EXAFS Fourier transform spectra of Ba ferrite ceramics and the nanoparticle species, together with best fits, as measured (black/solid, data; red/dotted, model) and after AAB removal (blue/dashed, data; magenta/short dotted, model).

L vacancy states. For the purpose of the AAB the exact shape of the resonance is not overly important; the mechanism of the Fourier transform requires only a good guess of its overall strength.

At this point a remark on the transferability of the AAB is necessary. The issue has been discussed before (Kodre *et al.*, 2001), with the general conclusion that the atomic absorption of an element is an (almost) exact AAB for EXAFS spectra of all forms of the element and its compounds, after the chemical shift of the absorption edge is taken into account, *i.e.* when the energy scale relative to the edge is used. The validity of the

Table 3
Constants of the Lorentzian $A(\Gamma^2/\{4[E-(E_3+\Delta E)]^2+\Gamma^2\})$ and the edge $A((1/2)+(1/\pi)\arctan\{[E-(E_3+\Delta E)]/(\Gamma/2)\})$ of the analytical approximation to the 4*d* contribution to the AAB.

	Lorentzian	Edge
ΔE (eV)	109	124
A	0.025	0.0076
Γ (eV)	12	2.2

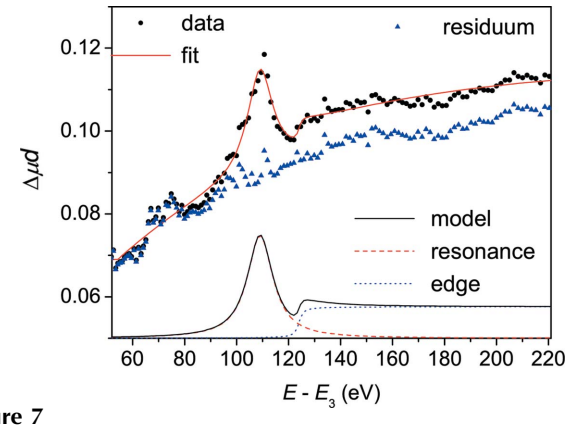

Figure 7
Analytic approximation to the Ba L_3 AAB. The model components (below), with addition of a simple exponential saturation term, are used to describe the 4*d* region in the experimental AAB.

conclusions rests on the fact that the EXAFS AAB comprises mostly coexcitations of the inner shells where the shake-up and shake-off processes prevail. Their fingerprints, *i.e.* tiny absorption edges and changes of slope, are insensitive to the changes in the valence orbitals of the atom. The coexcitations of the valence electrons, on the other hand, are highly variable from one chemical form to another, but they require much smaller energies and remain within the XANES region of the absorption spectrum.

The MPE resonances, no matter how deep in the EXAFS region, involve unoccupied bound orbitals in the final state, and are, accordingly, sensitive to the chemical state of the element. In this view, the AAB constructed from the absorption spectrum of the hydrated ion is perfectly transferable to the Ba ferrite, since in both states the Ba atom is surrounded by a full shell of oxygen atoms. The transferability is corroborated by the similarity of the L_3-edges, or rather by the similar relative strength of the white lines. To adapt the background for EXAFS spectra of samples with Ba neighbours of a different electron affinity, and hence a different edge profile, the amplitude of the resonance in the proposed analytical model can be corrected with the ratio of relative strengths of the respective white lines.

5. Conclusion

For certain series of elements in the periodic table, most notably for elements from Cs far into the lanthanide series, the AAB is known to contain a strong resonant contribution from the 4*d* coexcitation. The resonance falls in the middle of the

useful interval of k-space and cannot be eliminated by the standard spline routine. For elements like La and Ce, the possible loss of accuracy in the EXAFS analysis of weak structural signal was deemed so severe that the much less available K-edge EXAFS spectra with a smaller and more diffuse 4d resonance were resorted to (Fonda *et al.*, 1999). D'Angelo *et al.* (2008) have compared systematically the K and L EXAFS in the lanthanides in view of the effect of the 4d MPE, and found that the advantage of an untruncated k-interval in the K spectra outweighs the loss of resolution due to the large lifetime width. We have demonstrated that the problem can be solved within L_3 EXAFS and that good results can be obtained even from a very weak structural signal. The sharp 4d resonance contributes a Fourier transform extending over an extremely wide frequency interval, but with low amplitude. Consequently, its perturbation of any structural harmonic component is limited; the main effect is the loss of the overall quality of the fit whereby the estimated confidence intervals of the parameters and their correlations are increased. With this, the selectivity of the analysis against false models or unphysical ansatz components is diminished. The elimination of the AAB in the 4d region or just a simplest analytical model thereof, as shown above, can provide an effective remedy.

This work has been supported by the Slovenian Research Agency research programme P1-0112. We acknowledge the European Synchrotron Radiation Facility for provision of synchrotron experimental facilities (proposal HD-370) and we thank M. Ruffoni of beamline BM29 for support at the experiment.

References

D'Angelo, P., De Panfilis, S., Filipponi, A. & Persson, I. (2008). *Chem. Eur. J.* **14**, 3045–3055.
D'Angelo, P., Pavel, N. V. & Roccatano, D. (1996). *Phys. Rev. B*, **54**, 12129–12138.
Filipponi, A., Di Cicco, A. & Natoli, C. R. (1995). *Phys. Rev. B*, **52**, 15122–15134.
Filipponi, A., Ottaviano, L. & Tyson, T. A. (1993). *Phys. Rev. A*, **48**, 2098–2101.
Fonda, E., Andreatta, D., Colavita, P. E. & Vlaic, G. (1999). *J. Synchrotron Rad.* **6**, 34–42.
Ion, E.-D., Malič, B., Arčon, I., Padežnik Gomilšek, J., Kodre, A. & Kosec, M. (2010). *J. Eur. Ceram. Soc.* **30**, 569–575.
Jitschin, W. & Stotzel, R. (1998). *Phys. Rev. A*, **58**, 1221–1224.
Kodre, A., Arčon, I., Padežnik Gomilšek, J., Prešeren, R. & Frahm, R. (2002). *J. Phys. B*, **35**, 3497–3513.
Kodre, A., Padežnik Gomilšek, J., Arčon, I. & Aquilanti, G. (2010). *Phys. Rev. A*, **82**, 022513.
Kodre, A., Padežnik-Gomilšek, J., Arčon, I. & Prešeren, R. (1999). *J. Synchrotron Rad.* **6**, 306–307.
Kodre, A., Padežnik Gomilšek, J., Mihelič, A. & Arčon, I. (2006). *Radiat. Phys. Chem.* **75**, 188–194.
Kodre, A., Prešeren, R., Arčon, I., Padežnik Gomilšek, J. & Borowski, M. (2001). *J. Synchrotron Rad.* **8**, 282–284.
Kutzner, M. (2004). *Radiat. Phys. Chem.* **70**, 95–104.
Li, G., Bridges, F. & Brown, G. S. (1992). *Phys. Rev. Lett.* **68**, 1609–1612.
Makovec, D., Primc, D., Kodre, A., Šturm, S., Hanžel, D. & Drofenik, M. (2011). In preparation.
Mihelič, A., Kodre, A., Arčon, I., Padežnik Gomilšek, J. & Borowski, M. (2002). *Nucl. Instrum. Methods Phys. Res. B*, **196**, 194–197.
Obradors, X., Collomb, A., Pernet, M., Samaras, D. & Joubert, J. C. (1985). *J. Solid State Chem. B*, **56**, 171–181.
Padežnik Gomilšek, J., Arčon, I., De Panfilis, S. & Kodre, A. (2009). *Phys. Rev. A*, **79**, 032514.
Padežnik Gomilšek, J., Kodre, A., Arčon, I. & Hribar, M. (2003). *Phys. Rev. A*, **68**, 042505.
Padežnik Gomilšek, J., Kodre, A., Arčon, I., Loireau-Lozac'h, A. M. & Benazeth, S. (1999). *Phys. Rev. A*, **59**, 3078–3081.
Padežnik Gomilšek, J., Kodre, A., Arčon, I. & Prešeren, R. (2001). *Phys. Rev. A*, **64**, 22508.
Padežnik Gomilšek, J., Kodre, A., Bukovec, N. & Kozjek Škofic, I. (2004). *Acta Chim. Slov.* **51**, 23–32.
Prešeren, R., Kodre, A., Arčon, I. & Borowski, M. (2001). *J. Synchrotron Rad.* **8**, 279–281.
Primc, D., Makovec, D., Lisjak, D. & Drofenik, M. (2009). *Nanotechnology*, **20**, 315605.
Ravel, B. & Newville, M. (2005). *J. Synchrotron Rad.* **12**, 537–541.
Rehr, J. J. & Albers, R. C. (2000). *Rev. Mod. Phys.* **72**, 621–654.
Solera, J. A., Garcia, J. & Proietti, M. G. (1995). *Phys. Rev. B*, **51**, 2678–2686.
Žitnik, M., Kavčič, M., Bučar, K., Mihelič, A., Štuhec, M., Kokalj, J. & Szlachetko, J. (2007). *Phys. Rev. A*, **76**, 032506.